SCIENTIFIC REP🞓RTS

OPEN

Energy Dissipation Pathways in Few-Layer MoS$_2$ Nanoelectromechanical Systems

Bernard R. Matis, Brian H. Houston & Jeffrey W. Baldwin

Free standing, atomically thin transition metal dichalcogenides are a new class of ultralightweight nanoelectromechanical systems with potentially game-changing electro- and opto-mechanical properties, however, the energy dissipation pathways that fundamentally limit the performance of these systems is still poorly understood. Here, we identify the dominant energy dissipation pathways in few-layer MoS$_2$ nanoelectromechanical systems. The low temperature quality factors and resonant frequencies are shown to significantly decrease upon heating to 293 K, and we find the temperature dependence of the energy dissipation can be explained when accounting for both intrinsic and extrinsic damping sources. A transition in the dominant dissipation pathways occurs at $T \sim 110$ K with relatively larger contributions from phonon-phonon and electrostatic interactions for $T > 110$ K and larger contributions from clamping losses for $T < 110$ K. We further demonstrate a room temperature thermomechanical-noise-limited force sensitivity of ~8 fN/Hz$^{1/2}$ that, despite multiple dissipation pathways, remains effectively constant over the course of more than four years. Our results provide insight into the mechanisms limiting the performance of nanoelectromechanical systems derived from few-layer materials, which is vital to the development of next-generation force and mass sensors.

Nanoelectromechanical systems (NEMS) derived from stable, atomically thin and ultralightweight two-dimensional (2D) materials like graphene[1–3], the transition metal dichalcogenides (TMDs)[4, 5], and phosphorene[6] offer the prospect of coupling the mechanical degree of freedom to the unique properties of each material[7] thus creating a new class of mechanically active architectures with novel electro- and opto-mechanical capabilities. Mechanical energy dissipation is ubiquitous in all NEMS and sets a fundamental limit on the performance of these systems. Measurements of the temperature, T, dependent energy dissipation, Q^{-1} (where Q is the resonator quality factor), in graphene and monolayer WSe$_2$ NEMS show a substantial increase in Q^{-1} (over several decades) from liquid helium temperatures up to room temperature[1, 5]. Though Q has been shown to exceed 1.0×10^4 in these systems at cryogenic temperatures (~1.0×10^5 for graphene), the increase in mechanical energy dissipation with increasing T substantially reduces the Q values, which limits the room temperature force sensitivity of each resonator (since the limit of force sensitivity[2] $dF \propto (T/Q\omega)^{1/2}$, where $\omega = 2\pi f$ and f is the resonator frequency).

In this work, we use an all-optical setup to characterize the T dependence of Q^{-1} for few-layer MoS$_2$ NEMS, which allows us to determine the dissipation mechanisms responsible for the experimentally observed Q values from $T = 4.4$ K up to room temperature. A pulsed blue diode laser ($\lambda = 412$ nm) modulated at frequency, f, thermoelastically excites the resonator into resonance while the reflected light intensity of a red ($\lambda = 633$ nm) helium-neon laser is monitored to detect the resonator motion. In all instances, care is taken to avoid absorptive heating and dynamical photothermal back-action from the lasers, by limiting the amount of laser power delivered to the sample[5]. All measurements are carried out in vacuum (pressure ~10^{-6} Torr), minimizing energy dissipation due to gas friction (see the Supplementary Information). The sample is mounted in front of an optical window within a variable temperature helium cryostat.

Room temperature measurements demonstrate fundamental and higher order modes in the 10–100 MHz range with measured Q on the order of ~100. Upon cooling to 4.4 K, Q reaches values on the order of 1.0×10^4 while the fundamental mode increases in frequency by ~10 MHz. At 4.4 K, the experimentally determined Young's Modulus, E, of the few-layer MoS$_2$ resonator is ~178 GPa, which is within experimental error of the values obtained for single- and bi-layers, $E \sim 270 \pm 100$ GPa and $E \sim 200 \pm 60$ GPa, respectively[8]. We find that it is

Naval Research Laboratory, Code 7130, Washington, DC, 20375, United States. Correspondence and requests for materials should be addressed to B.R.M. (email: bernard.matis@nrl.navy.mil)
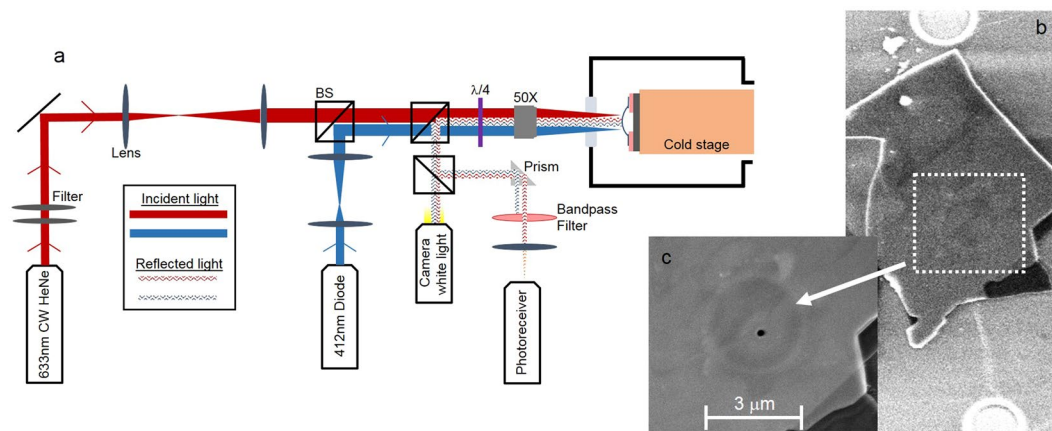
Figure 1. Optical interferometer and MoS$_2$ resonator. (**a**) Schematic showing the optical interferometer, and sample mount within the variable temperature cryostat. BS = Beam Splitter. $\lambda/4$ = quarter-wave plate. (**b** and **c**) Scanning electron microscopy images of one of the MoS$_2$ resonators tested within this study. The observable hole near the center of the resonator in (**c**) was made by ion milling with a focused ion beam to test the impact of trapped air beneath the MoS$_2$ on the overall mechanical properties of the resonator.
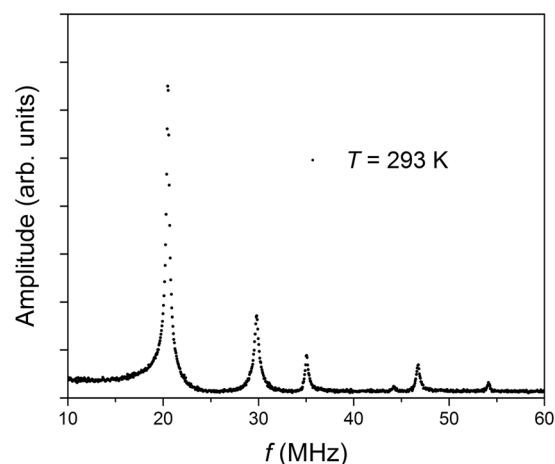

Figure 2. Room temperature mechanical resonance spectrum. Amplitude as a function of frequency, f, for the 17-nm-thick MoS$_2$ resonator showing the fundamental mode ($f \sim 21.8$ MHz) and higher-order modes.

necessary to account for both intrinsic (phonon-phonon interactions) and extrinsic (clamping and electrostatic coupling to the substrate) sources of energy dissipation in order to explain the observed temperature dependence of Q^{-1} while thermoelastic dissipation and dissipation due to surface losses do not play a significant role. The experimentally determined functional form of $Q^{-1}(T)$ indicates a transition in the dominant energy dissipation pathways at $T \sim 110$ K with relatively larger contributions to $Q^{-1}(T)$ from phonon-phonon and electrostatic interactions in the high temperature regime and larger contributions from clamping losses in the low temperature regime. Despite the presence of multiple dissipation pathways, measurements of the room temperature product $Q\omega$ result in a force sensitivity of ~ 8 fN/Hz$^{1/2}$ that is found to remain constant over the course of over four years, suggesting long-term durability and functionality of these few layer TMD NEMS.

Results

Optical characterization. The optical interferometer used in our experiments is shown schematically in Fig. 1a. Scanning electron micrographs of one of the circular, drumhead resonators used in this study are shown in Fig.' s1b,c. Few-layer MoS$_2$ flakes were mechanically exfoliated from bulk MoS$_2$ crystals onto a SiO$_2$/(doped) Si substrate with predefined circular trenches etched out of the SiO$_2$. Atomic force microscopy was used to determine flake thickness. A total of three resonators were tested in this study, all of which showed the same qualitative behavior, and we present data from one representative resonator.

Figure 2 shows the measured mechanical amplitude versus frequency at room temperature for a 17-nm-thick (~ 26 monolayers) MoS$_2$ resonator with a radius $r \sim 3\,\mu$m. The choice to study few-layer resonators was for several reasons: particularly, for comparing energy dissipation pathways in the transition from bulk to single-atomic
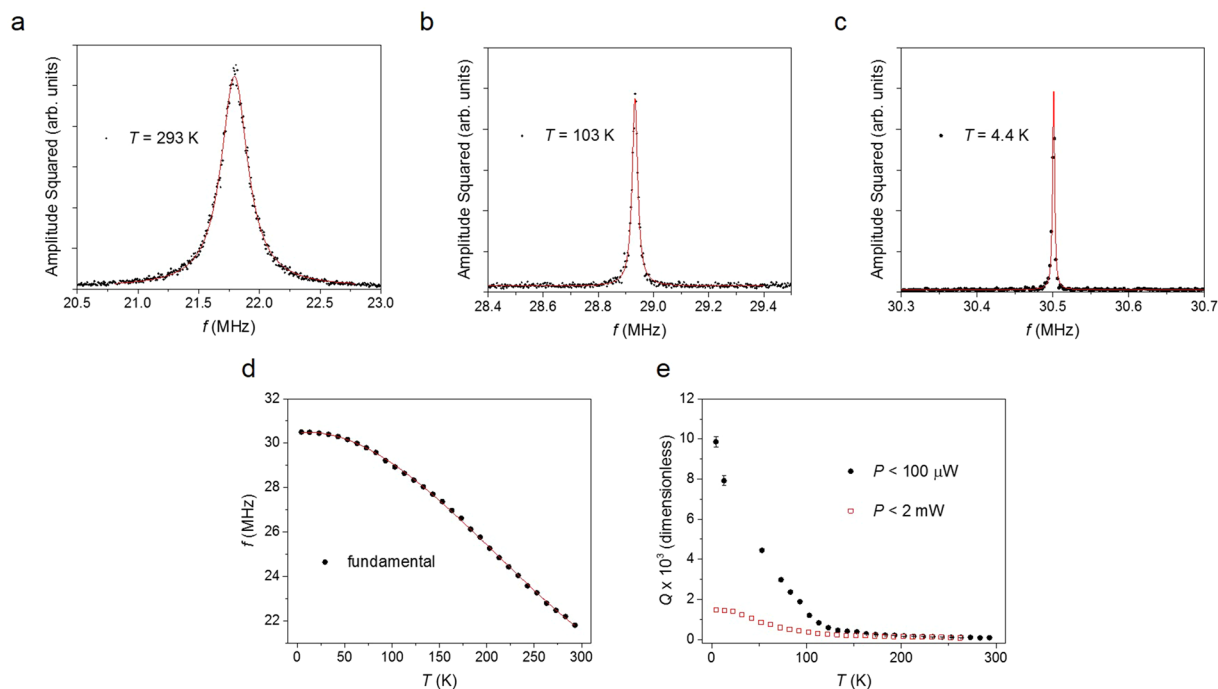
Figure 3. Temperature dependence of the MoS$_2$ resonator fundamental mode. (**a–c**) Square of the amplitude as a function of frequency, f, for varying temperature, T. The solid red lines are Lorentzian fits to the data. (**d**) Fundamental frequency as a function of T. The solid red line is a fit to a third-order polynomial, which is used in the subsequent data analysis for determining energy dissipation pathways. (**e**) Resonator quality factor, Q, as a function of T for varying laser power, P.

layer material, and to determine whether a few-layer MoS$_2$ resonator could in fact possess the same exceptional mechanical properties as those of its single-layer counterparts (e.g. high Q) while simultaneously combining long-term durability against energy dissipation due to surfaces losses (e.g. from physisorbed species). For the data shown in Fig. 2, the fundamental mode is observed at $f \sim 21.8$ MHz, which shows the largest mechanical amplitude as well as higher-order vibrational modes. For the remainder of our temperature-dependent data analysis we focus our discussion on the fundamental mode. Determination of the resonant frequency and full-width-at-half-maximum, Γ, which is used in the determination of the quality factor $Q = f/\Gamma$, is done through a Lorentzian fitting of the square of the measured amplitude versus frequency.

Figures 3a–c show the amplitude squared versus frequency for three separate temperatures (293 K, 103 K and 4.2 K), which include the Lorentzian fits used to extract f and Γ. Lorentzian fits to the data shown in Fig. s3a–c yield $f \sim 21.8$ MHz and $Q \sim 82 \pm 1$ at $T = 293$ K, and $f \sim 31$ MHz and $Q \sim 9,857 \pm 271$ at $T = 4.4$ K. The increase in Q and f with decreasing T is consistent with prior studies on graphene and monolayer MoS$_2$ and WSe$_2$ NEMS[1, 5]. The strong temperature dependence of f has been associated with the thermal expansion of the resonator. Figure 3d shows the temperature dependence of the fundamental frequency, determined through Lorentzian fittings like those shown in Fig. s3a–c, along with a fit to a third order polynomial (see the Supplementary Information). The third order polynomial is used in the subsequent data analysis (see below) to accurately fit the temperature dependence of the experimentally observed energy dissipation (which can depend on f). Furthermore, the frequency modes for a circular plate resonator (in the limit of zero tension) can be expressed as[9]

$$f_{mn} = (\pi t/4r^2)\sqrt{E/3\rho(1 - s^2)}\,(\beta_{mn})^2$$

where $t \sim 17$ nm is the plate thickness, E is the Young's modulus, $\rho \sim 5,060$ kg/m^3 is the resonator mass density[10], $s = 0.27$ is the Poisson's ratio for bulk MoS$_2$[11], and β_{mn} is the nth root of the mth-order Bessel function (here, we use $\beta_{01} = 2.4048$ when considering the fundamental mode). At $T = 4.4$ K and with $f \sim 31$ MHz we find $E \sim 178$ GPa, which is in reasonable agreement with stretching and breaking results of few layer MoS$_2$ films[8].

Throughout our experiments care was taken to avoid absorptive heating and dynamical photothermal back-action, as well as to operate within the linear regime away from any non-linear Duffing behavior. Upon cooling to 4.4 K, maximal laser power, P, induced observable Duffing nonlinearities in the resonator amplitude versus f[12, 13]. At 4.4 K, before capturing the data shown in Fig. 3, the laser power of each laser was reduced well below the minimum threshold required to observe Duffing behavior, toward the minimum power limit beyond which no resonance could be observed in the frequency spectrum, and to the point at which we perceived no observable changes in f and Γ. Figure 3e shows Q as a function of T for before and after this reduction in laser power. The power values given in the Fig. 3e legend represent upper limits, however laser power delivered to the
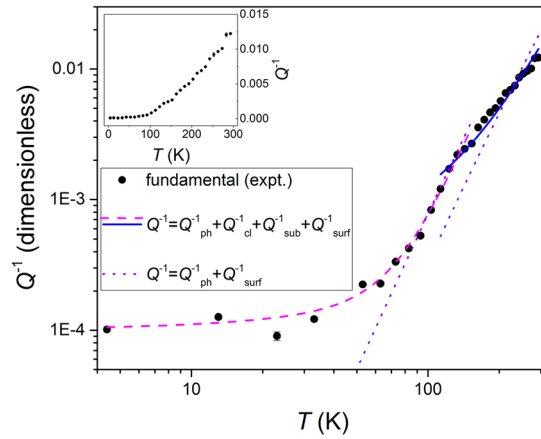
Figure 4. Temperature dependence of the energy dissipation. Inverse quality factor (energy dissipation), Q^{-1}, as a function of temperature, T. The solid black circles are the experimental data determined from measurements of the fundamental mode temperature dependence. The solid blue and dashed magenta lines are fits to the experimental data for $T > 110\,\text{K}$ and $T < 110\,\text{K}$, respectively, which take into account four dissipation pathways: Q^{-1}_{ph} = phonon-phonon dissipation, Q^{-1}_{cl} = clamping dissipation, Q^{-1}_{sub} = dissipation from electrostatic interactions with the substrate, and Q^{-1}_{surf} = surface dissipation. The dotted violet lines are fits to the data within the high and low temperature ranges that only take into account Q^{-1}_{ph} and Q^{-1}_{surf}. Inset: Q^{-1} versus T on a linear scale. The y-axis units are dimensionless.

sample is lower (see Methods). The data in Fig. 3e demonstrates that under minimal laser power conditions, Q values reaching 1.0×10^4 can be achieved in these few-layer resonators at cryogenic temperatures.

Dissipation mechanisms. Measurements of $Q^{-1}(T)$ allow us to identify the main causes of energy dissipation within the studied MoS$_2$ NEMS, and the experimentally determined $Q^{-1}(T)$ is shown in Fig. 4 (solid black circles). We identify two separate regimes for $Q^{-1}(T)$ with a transition occurring at $T \sim 110\,\text{K}$. Upon cooling, $Q^{-1}(T)$ falls approximately an order of magnitude between 293 K and 110 K, with measured $Q^{-1}(T)$ values of ~ 0.01 and $\sim 1 \times 10^{-3}$, respectively. For $T < 110\,\text{K}$, we find that $Q^{-1}(T)$ saturates to values of $\sim 1.0 \times 10^{-4}$ at the lowest temperatures, which results in quality factors as high as 10,000 at 4.4 K. The observed transition in the functional form of $Q^{-1}(T)$ near $T \sim 110\,\text{K}$ suggests that different dissipation pathways govern the energy dissipation within the high and low temperature regimes.

We consider multiple energy dissipation mechanisms in an effort to explain the experimentally determined functional form of $Q^{-1}(T)$. Dissipation due to phonon-phonon interactions, $Q^{-1}_{ph}(T)$, within the Akheiser regime[14, 15] can be expressed as

$$Q^{-1}_{ph}(T) = \frac{C_v \gamma^2 T}{\rho v^2} \frac{\omega \tau_{ph}}{1 + \omega^2 \tau_{ph}^2}$$

where $\gamma \sim 1.1$ is Grüneisen's constant[16] for MoS$_2$, C_v is the heat capacity per unit volume, v is the sound velocity within the MoS$_2$ and τ_{ph} the phonon relaxation time. For multilayer MoS$_2$[17], $v \sim 7.11 \times 10^3\,\text{m/s}$, which corresponds to $\lambda \sim 326\,\mu\text{m}$ at $f \sim 21.8\,\text{MHz}$. The Akheiser regime is applicable in our samples since $\lambda \gg L_{ph}$ (where $L_{ph} \sim 200\,\text{nm}$ is the phonon mean free path[18]) and $1/\tau_{ph} \gg \omega$ where $\tau_{ph} = 3\kappa/C_v v^2 \sim 2\,\text{ps}$ with $\kappa \sim 52\,\text{W/Km}$ is the few-layer MoS$_2$ thermal conductivity[19] and the heat capacity is ref. 20 $C_v \sim 1.89 \times 10^6\,\text{J/m}^3\text{K}$ (see the Supporting Information for further discussion on the Akheiser regime). Within this regime, the oscillatory sound wavelength perturbs the phonon distribution from the equilibrium Planck form, while the restoration of the phonon gas to thermal equilibrium is accompanied by dissipation in the resonator. We further take into account clamping losses (energy radiated away from the resonator into the substrate), Q^{-1}_{cl}, which we take to be independent of temperature. Prior works have studied clamping losses in detail and have shown that such dissipation is temperature independent and arises purely from the geometry of the system[21, 22].

We also take into account dissipation due to electrostatic interactions between the charges in the resonator and the doped silicon substrate, $Q^{-1}_{sub}(T)$. For the case of graphene, it has been shown theoretically that the room temperature dissipation is dominated by ohmic losses at the graphene and the metallic gate[21]. Here, the charge carriers within the resonator induce a time-dependent potential on the backgate, thus creating electron-hole pairs within the resonator and/or backgate. Electron-hole generation processes such as these results in energy dissipation, which can be the dominant energy dissipation pathway for 2D graphene-based NEMS. In this case, $Q^{-1}_{sub}(T)$ should increase linearly with temperature[21]. We note the importance of incorporating the linear in T term to the overall dissipation observed within our studied NEMS, as its inclusion is necessary for accurately describing the observed functional form of $Q^{-1}(T)$. Unlike the case of monolayer graphene, however, we do not expect $Q^{-1}_{sub}(T)$ to be the dominant dissipation pathway within our few-layer resonators due to screening of the charge carriers within few-layer MoS$_2$.

Room temperature measurements on multilayer MoS_2 resonators have demonstrated a decrease in the quality factor with an increase in the surface to volume ratio[4], which indicates a contribution from surface-related dissipation to the overall $Q^{-1}(T)$. Therefore, we account for surface related dissipation using the known expression[23]

$$Q_{surf}^{-1}(T) = \frac{V_{monolayer}}{V} \frac{E\alpha^2 T}{C_p} \frac{\omega\tau_s}{1 + \omega^2\tau_s^2}$$

where $E \sim 178\,GPa$ is the experimentally determined Young's Modulus, $\alpha \sim 1 \times 10^{-6}$ is the MoS_2 average thermal expansion coefficient[24], we assume $C_p = C_v \sim 1.89 \times 10^6\,J/m^3\,K$, and $\tau_s = a^2 C_p/\kappa$ where a is the average crystallite size taken to be the diameter of the resonator (assuming surface-related effects across the entire resonator surface). The ratio $V_{monolayer}/V$ represents the ratio between the volumes of the damaged layer and the resonator as a whole and we assume the damaged layer to be the top MoS_2 layer of the resonator, which is the layer most susceptible to physisorbed species.

In comparing these dissipation models to our data, we use the experimentally determined $f(T)$ in determining $\omega(T)$ and further take into account the temperature dependence of α, C and κ. For $T < \Theta_D$ where $\Theta_D \sim 250\,K$ is the few-layer MoS_2 Debye temperature[25], we use $\alpha \propto T^3$, $\kappa \propto T^3$ and $C_v \propto T^3$ as the functional form of the temperature dependence of these quantities[26]. We find that $Q^{-1}(T) = Q_{ph}^{-1}(T) + Q_{cl}^{-1} + Q_{sub}^{-1}(T) + Q_{surf}^{-1}(T)$ can accurately account for the observed temperature dependence of the energy dissipation within the high and low temperature regimes (solid blue and dashed magenta lines in Fig. 4, respectively), indicating contributions from each of these dissipation pathways. The two additional fits in Fig. 4, corresponding to the dotted violet lines, demonstrate that $Q^{-1}(T) = Q_{ph}^{-1}(T) + Q_{surf}^{-1}(T)$ cannot alone explain the observed $Q^{-1}(T)$ within the high and low temperature ranges and that accounting for clamping and electrostatic-related losses is necessary. However, from the fittings to the data shown in Fig. 4 (solid blue and dashed magenta lines) we do find that the relative contributions from each dissipation pathway changes between the two temperature regimes. For $T > 110\,K$, we find that the largest contributions to $Q^{-1}(T)$ are from $Q_{ph}^{-1}(T)$ and $Q_{sub}^{-1}(T)$, while for $T < 110\,K$ the largest contributions to $Q^{-1}(T)$ are from Q_{cl}^{-1}. Physically, this corresponds to a transition to clamping related losses for $T < 110\,K$ as the MoS_2 phonon and carrier density populations are reduced with decreasing temperature. We also find negligible contributions from $Q_{surf}^{-1}(T)$ within both the high and low temperature regimes, which indicates that losses due to physisorbed species, for example, are negligible. Additionally, prior works on InAs nanowires[27] have demonstrated that energy dissipation due to clamping related losses results in a total measured dissipation on the order of 10^{-4} at low temperatures, which is consistent with our results that $Q^{-1}(T) \sim Q_{cl}^{-1} \sim 10^{-4}$ at $T = 4.4\,K$ (additional detailed information regarding the data analysis can be found in the Supporting Information). The results for few-layer MoS_2 NEMS are strikingly different than the theoretical predictions for the dominant loss mechanisms in single layer graphene[21] (which predict $Q_{sub}^{-1}(T)$ to dominate) and semiconductor resonators with micron-scale thickness[28] (which show that thermoelastic loss dominates).

It has been demonstrated previously that thermoelastic damping (dissipation stemming from the transduction of elastic energy into thermal energy via a temperature gradient established between compressed and expanded regions of the resonator) is the dominant source of dissipation in semiconductor microscale resonators[28] with $1.5\,\mu m$ thickness. According to the Zener theory for thermoelastic damping, the dissipation is expressed as

$$Q_{Ze}^{-1}(T) = \frac{E\alpha^2 T}{C_p} \frac{\omega\tau_{th}}{1 + \omega^2\tau_{th}^2}$$

where α is the thermal expansion coefficient, C_p is the constant stress heat capacity, and $\tau_{th} = t^2 C_p/\pi^2 \kappa$ is the thermal relaxation time. For our samples, $1/\tau_{th} \sim 9 \times 10^{11}\,Hz$, which is 4 orders or magnitude larger than the fundamental frequency associated with our resonator. Within the thermoelastic model, the dissipation highly depends upon excitation frequency with $Q_{Ze}^{-1}(T) \sim 0$ when the product $\omega\tau_{th}$ is outside of the range[14] $0.01 \leq \omega\tau_{th} \leq 100$. In our samples, $\omega\tau_{th} \sim 2.3 \times 10^{-5}$, which suggests that thermoelastic dissipation is not a dominant dissipation pathway within these few-layer systems.

Long-term durability. TMDs are seen as promising 2D candidates in an effort to replace or augment current semiconducting technologies utilizing Si, Ge, and other III-V compounds. Practical applications rely on the ability to develop device architectures with long-term durability and stability. It is known that the electrical performance of multilayer MoS_2 transistors is unstable under ambient conditions, and that the adsorption of oxygen and/or water from the environment can substantially impact the electronic properties[29]. The same holds true for chemically modified graphene transistors[30]. In the case of phosphorene, degradation of the material due to photoassisted oxidation has been shown to occur on the timescale of several hours, which markedly hinders its technological applicability[31]. In terms of TMDs-based NEMS, however, we find that a few-layer MoS_2 resonator is capable of operating over the duration of years without loss of force sensitivity and functionality, which affords significant promise in the applicability of such mechanically-active architectures.

Figure 5 shows the normalized measured mechanical amplitude versus frequency at room temperature taken more than 4 years apart (data represented by the solid black circles is from the same data set shown in Fig. 2). After the initial exfoliation and measurements (8–2–2012 in Fig. 5), the sample was placed in a nitrogen-purged dry box at $<20\%$ humidity level. The quality factor decreased from ~96 to ~82 over the course of the 4 years and 3 months with only small changes in the product $Q\omega$, which decreased from ~1.5×10^{10} to ~1.1×10^{10}. The limit on the resonator force sensitivity is given by
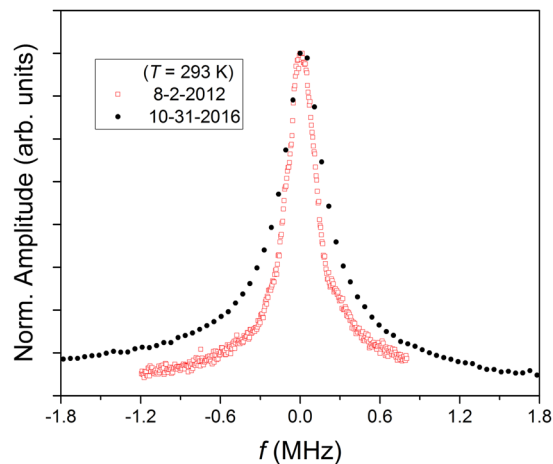
Figure 5. Time dependence of the fundamental mode. Normalized amplitude as a function of f-f_O, where f_O is the fundamental frequency, measured at room temperature and at two separate times: after initial exfoliation (8-2-2012) and nearly 4 years and 3 months later (10-31-2016).

$$dF = \left(4\kappa_{eff}k_B T/Q\omega\right)^{1/2},$$

where $\kappa_{eff} = m_{eff}\omega^2 = \pi r^2 t\rho\omega^2$ is the effective spring constant and k_B is Boltzmann's constant. We calculate the force sensitivity change from 8 fN/Hz$^{1/2}$ to 8.2 fN/Hz$^{1/2}$ between the time-dependent data sets shown in Fig. 5 indicating that the force sensitivity of the resonator remained effectively constant over the duration of more than 4 years.

In summary, we have measured the temperature dependence of the energy dissipation for few-layer MoS$_2$ NEMS. Our results indicate that both intrinsic (phonon-phonon interactions) and extrinsic (clamping and electrostatic coupling to the substrate) dissipation sources contribute to the overall observed energy dissipation. We find that for $T > 110$ K the largest contributions to the overall dissipation are related to phonon-phonon and electrostatic interactions, while for $T < 110$ K the largest contributions to the dissipation are related to clamping losses. These results are markedly different from single-layer NEMS and micron-scale semiconductor systems, and results in a new regime due to the few-layer nature of the MoS$_2$ NEMS. We further demonstrate the mechanical durability and nearly constant force sensitivity of the MoS$_2$ NEMS over the time span of more than 4 years. Our results are important for understanding the fundamental limitations of few-layer NEMS at room temperature, and for the long-term applications in force and mass sensing and opto-mechanical/electro-mechanical transducers derived from few-layer materials.

Methods

Device Fabrication. Few-layer MoS$_2$ flakes were mechanically exfoliated from bulk MoS$_2$ crystals onto a SiO$_2$/Si substrate with predefined circular trenches etched out of the SiO$_2$. Prior to the exfoliation, standard optical lithography and reactive ion etching were used to define the trenches in the SiO$_2$. No subsequent patterning or annealing was carried out following the exfoliation. A Bruker Dimension FastScan AFM was used to determine the thickness of the exfoliated flakes.

Optical setup. The frequency spectrum of the blue diode laser, which is used for resonator excitation, is controlled with a spectrum analyzer. The reflected light intensity of the red laser, which is monitored to detect the resonator motion, is focused onto a low-noise photoreceiver after being passed through a narrow-band filter where blue wavelengths are blocked from reaching the photoreceiver. The output of the photoreceiver is measured with the spectrum analyzer thus allowing for a lock-in technique to detect the resonator motion. The cryostat is manipulated using an x-y-z stage, which allows for 250 nm precision. Laser power is recorded using a Newport Corporation power meter with a calibrated photodiode sensor.

Time-dependent measurements. We point out that, with the exception of the data from 8-2-2012 presented in Fig. 5, all other data sets within this article were taken on or after 10-31-2016.

Data availability. The datasets generated during and/or analyzed during the current study are available from the corresponding author on reasonable request.

References

1. Chen, C. *et al.* Performance of monolayer graphene nanomechanical resonators with electrical readout. *Nature Nanotechnol.* **4**, 861–867 (2009).
2. Bunch, J. S. *et al.* Electromechanical resonators from graphene sheets. *Science* **315**, 490–493 (2007).
3. Robinson, J. T. *et al.* Wafer-scale reduced graphene oxide films for nanomechanical devices. *Nano Lett.* **8**(10), 3441–3445 (2008).

4. Lee, J., Wang, Z., He, K., Shan, J. & Feng, P. X.-L. High frequency MoS$_2$ nanomechanical resonators. *ACS Nano* **7**(7), 6086–6091 (2013).
5. Morell, N. *et al.* High quality factor mechanical resonators based on WSe$_2$ monolayers. *Nano Lett.* **16**, 5102–5108 (2016).
6. Wang, Z. & Feng, P. X.-L. Design of black phosphorus 2D nanomechanical resonators by exploiting the intrinsic mechanical anisotropy. *2D Mater.* **2**, 021001 (2015).
7. Butler, S. Z. *et al.* Progress, challenges, and opportunities in two-dimensional materials beyond graphene. *ACS Nano* **7**(4), 2898–2926 (2013).
8. Bertolazzi, S., Brivio, J. & Kis, A. Stretching and breaking of ultrathin MoS$_2$. *ACS Nano* **5**(12), 9703–9709 (2011).
9. Blevins, R. D. *Formulas for Natural Frequency and Mode Shape*. Krieger Publishing Company: Malabar, FL, pp 226, 240 (1979).
10. Worsley, M. A. *et al.* Ultralow density, monolithic WS$_2$, MoS$_2$, and MoS$_2$/graphene aerogels. *ACS Nano* **9**(5), 4698–4705 (2015).
11. Feldman, J. L. Elastic constants of 2h-MoS$_2$ and 2h-NbSe$_2$ extracted from measured dispersion curves and linear compressibilities. *J. Phys. Chem. Solids* **37**, 1141–1144 (1976).
12. Aldridge, J. S. & Cleland, A. N. Noise-enabled precision measurements of a Duffing nanomechanical resonator. *Phys. Rev. Lett.* **94**, 156403 (2005).
13. Eichler, A. *et al.* Nonlinear damping in mechanical resonators made from carbon nanotubes and graphene. *Nature Nanotechnol* **6**, 339–342 (2011).
14. Cleland, A. N. *Foundations of Nanomechanics. From Solid-State Theory to Device Applications*. Springer-Verlag Berlin Heidelberg: New York, NY, pp 282–289 (2003).
15. Braginsky, V. B., Mitrofanov, V. P. & Panov, V. I. *Systems with Small Dissipation*. The University of Chicago Press: Chicago, IL, pp 11–12 (1985).
16. Conley, H. J. *et al.* Bandgap engineering of strained monolayer and bilayer MoS$_2$. *Nano Lett.* **13**, 3626–3630 (2013).
17. Ge, S. *et al.* Coherent longitudinal acoustic phonon approaching THz frequency in multilayer molybdenum disulfide. *Sci. Rep.* **4**, 5722 (2014).
18. Gu, X., Li, B. & Yang, R. Layer thickness-dependent phonon properties and thermal conductivity of MoS$_2$. *J. Appl. Phys.* **119**, 085106 (2016).
19. Yan, R. *et al.* Thermal conductivity of monolayer molybdenum disulphide obtained from temperature-dependent Raman spectroscopy. *ACS Nano* **8**(1), 986–993 (2014).
20. Liu, J., Choi, G.-M. & Cahill, D. G. Measurement of the anisotropic thermal conductivity of molybdenum disulphide by the time-resolved magneto-optic Kerr effect. *J. Appl. Phys.* **116**, 233107 (2014).
21. Seoánez, C., Guinea, F. & Castro Neto, A. H. Dissipation in graphene and nanotube resonators. *Phys. Rev. B* **76**, 125427 (2007).
22. Cross, M. C. & Lifshitz, R. Elastic wave transmission at an abrupt junction in a thin plate with application to heat transport and vibrations in mesoscopic systems. *Phys. Rev. B* **64**, 085324 (2001).
23. Braginsky, V. B., Mitrofanov, V. P. & Panov, V. I. *Systems with Small Dissipation*. The University of Chicago Press: Chicago, IL, pp 21–23 (1985).
24. Murray, R. & Evans, B. L. The thermal expansion of 2H-MoS$_2$ and 2H-WSe$_2$ between 10 and 320 K. *J. Appl. Cryst.* **12**, 312–315 (1979).
25. Liu, Y. *et al.* Thermally driven (Mo, W)-(S$_2$, Se$_2$) phonon and photon energy relaxation dynamics. *J. Phys. Chem. C* **119**, 25071–25076 (2015).
26. Ashcroft, N. W. & Mermin, N. D. *Solid State Physics*. Saunders College Publishing: Orlando, FL, pp 458–459, 493, 504 (1976).
27. Mathew, J. P. *et al.* Nanoscale Electromechanics to Measure Thermal Conductivity, Expansion, and Interfacial Loss. *Nano Lett.* **15**, 7621–7626 (2015).
28. Metcalf, T. H., Pate, B. B., Photiadis, D. M. & Houston, B. H. Thermoelastic damping in micromechanical resonators. *Appl. Phys. Lett.* **95**, 061903 (2009).
29. Cho, K. *et al.* Electric stress-induced threshold voltage instability of multi-layer MoS$_2$ field effect transistors. *ACS Nano* **7**(9), 7751–7758 (2013).
30. Matis, B. R. *et al.* Surface doping and band gap tunability in hydrogenated graphene. *ACS Nano* **6**(1), 17–22 (2012).
31. Favron, A. *et al.* Photooxidation and quantum confinement effects in exfoliated black phosphorus. *Nature Mater.* **14**, 826–833 (2015).

Author Contributions

B.R.M., J.W.B., and B.H.H. conceived the experiments. B.R.M. and J.W.B. fabricated the devices, performed the experiments, and analyzed the data. B.R.M., J.W.B. and B.H.H. wrote the manuscript.

Additional Information

Supplementary information accompanies this paper at doi:10.1038/s41598-017-05730-1

Competing Interests: The authors declare that they have no competing interests.

Publisher's note: Springer Nature remains neutral with regard to jurisdictional claims in published maps and institutional affiliations.